eLIFE
elifesciences.org

RESEARCH ARTICLE

Figures and figure supplements

TORC2-Gad8-dependent myosin phosphorylation modulates regulation by calcium

Karen Baker *et al*

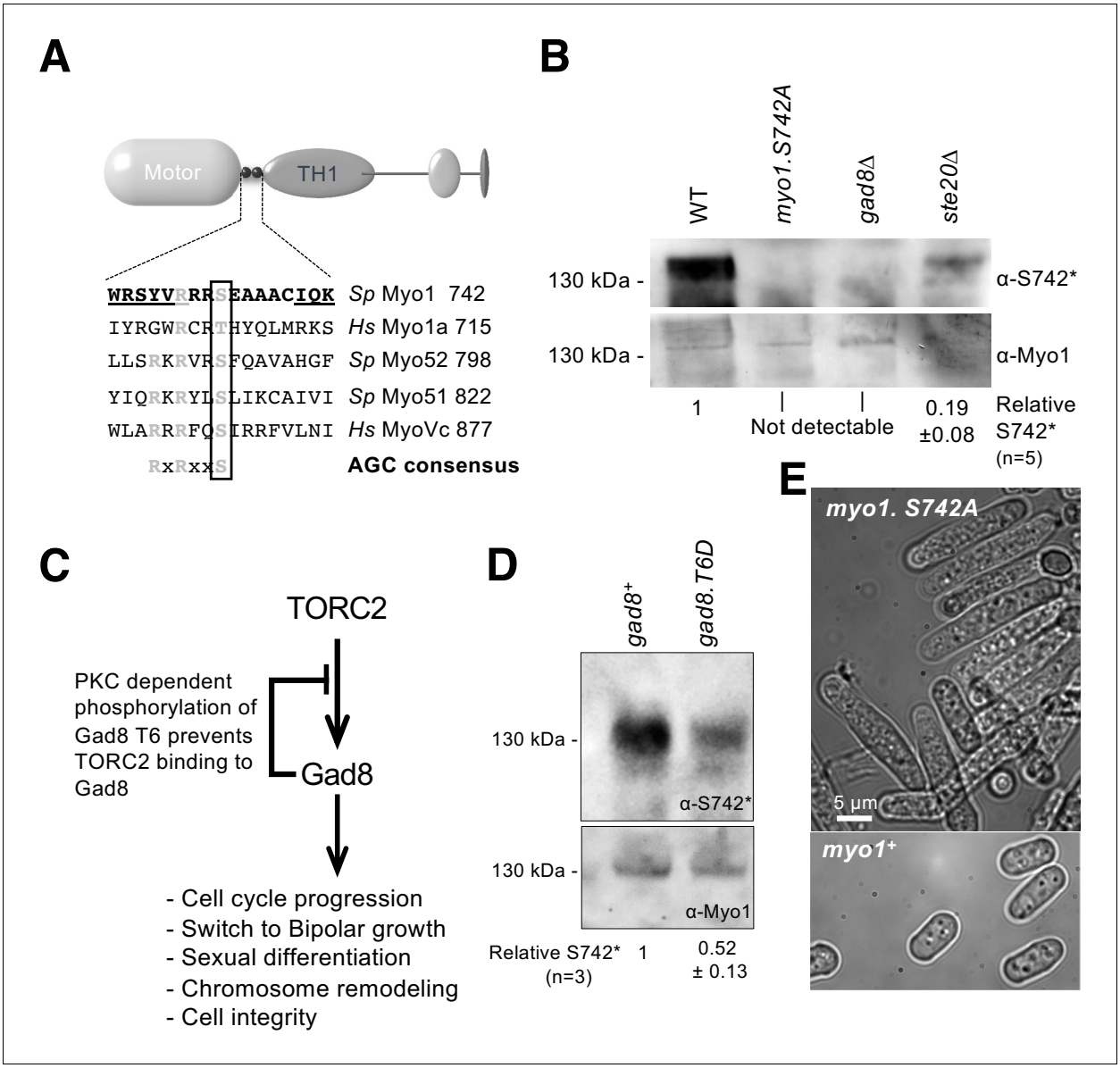

Figure 1. Myo1 serine 742 phosphorylation is TORC2 dependent. (**A**) The sequence alignment of myosin IQ regions highlights an AGC kinase consensus sequence that is conserved in class I and V myosins. Underlined residues are those within IQ motifs. (**B**) Western blots of extracts from *myo1*$^{+}$, *myo1-S742A*, *gad8*Δ and *ste20*Δ cells probed with phospho-specific anti-Myo1^{S742} (upper panel) and anti-Myo1 (lower panel) antibodies demonstrate antigen specificity and a Myo1^{S742} phosphorylation-state dependence upon the TORC2–Gad8 pathway. Ponceau staining was used to monitor equal loading. Relative Myo1^{S742} phosphorylation levels were calculated from five independent equivalent experiments (mean ± sd). (**C**) A schematic of the TORC2–Gad8 signaling pathway. (**D**) Myo1^{S742} phosphorylation is reduced in *gad8.T6D* cells, which have reduced Gad8 kinase activity. Relative Myo1^{S742} phosphorylation levels were calculated from three independent equivalent experiments (mean ± sd). (**E**) Nitrogen-starved wildtype (WT) and *myo1.S742A* cells. In contrast to WT cells, in which growth arrests, *myo1.S742A* cells continue to grow upon nitrogen-starvation-induced G_1 arrest. Scale bar: 5 µm.

DOI: https://doi.org/10.7554/eLife.51150.003

Figure 2. In vitro characterization of interactions between Myo1 and Cam1. (**A**) Predicted models of the CyPet–Cam1–YPet FRET reporter protein (Cam1–FRET) in the absence (upper panel) and presence (lower panel) of Ca^{2+}. (**B**) Predicted models of the CyPet–Myo1^{IQ12}–YPet FRET reporter protein (Myo1IQ12–FRET) in the absence (upper panel) or presence (lower panel) of calmodulin binding (Cypet, cyan; Cam1, yellow; YPet, green; IQ domain,

Figure 2 continued on next page

Figure 2 continued

magenta). (**C**) pCa curve plotting Ca^{2+}-dependent changes in the acceptor fluorescence (plotted as ΔYPet signal) of the Cam1–FRET protein (red), Cam1 association with $Myo1^{IQ12}$-FRET (black) and change in the fluorescence of IAANS-labelled Cam1–T6C (inset). (**D**) Transient curves of changes in Quin2 fluorescence induced by Ca^{2+} release from Cam1 (red) (with three exponential fit best fit (black)) and from Cam2 (blue) illustrate that only Cam1 associates with Ca^{2+}. (**E**) Curves plotting Cam1- (black) and Cam2-dependent (red) changes of the FRET donor signal of Myo1–FRET proteins containing single IQ domains (IQ1, empty shapes; IQ2, filled shapes) each show that CaM associates with IQ1 but not with an equivalent single IQ2 motif region. (**F**) Curves plotting Cam1- (squares and triangles) and Cam2-dependent (circles and diamonds) changes in the FRET donor signal of either 0.5 μM wild type (black and red) or S742D phosphomimetic (blue) $Myo1^{IQ12}$–FRET proteins show that although phosphorylation does not significantly impact Cam1 binding, it results in a drop of about 50% in Cam2 interaction. (**G**) Spectra of 0.5 μM $Myo1^{IQ12}$–FRET reporter alone (grey line) or of 0.5 μM $Myo1^{IQ12}$–FRET reporter mixed with 10 μM saturating concentrations of: Cam1 + Ca^{2+} (black dotted line), Cam1 – Ca^{2+} (black solid line), Cam2 + Ca^{2+} (red dotted line), or Cam1 – Ca^{2+} (red solid line).

DOI: https://doi.org/10.7554/eLife.51150.004

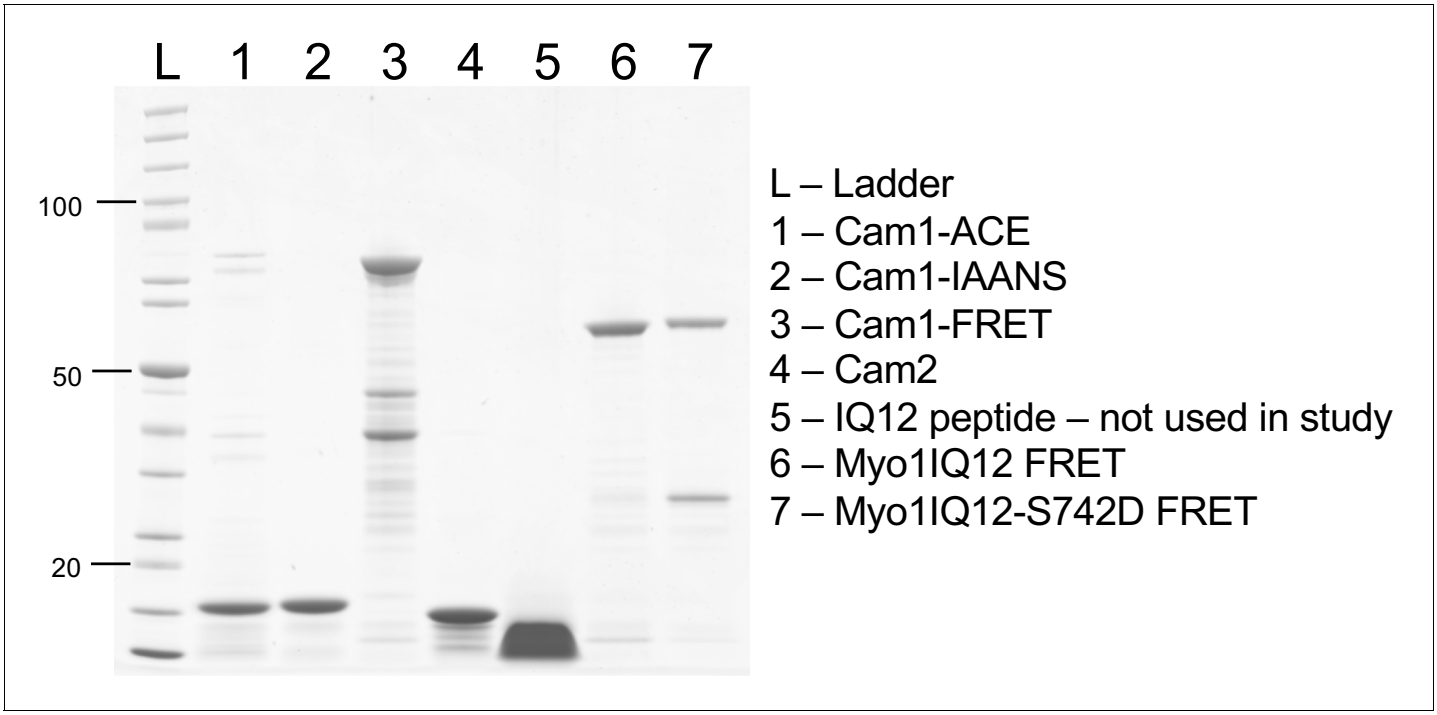

Figure 2—figure supplement 1. Purified proteins used during in vitro studies. Coomassie-stained SDS-PAGE gel of recombinant proteins expressed and purified during this study. From left to right, the lanes contain (**L**) protein standard; (1) Nt-acetylated Cam1; (2) Nt-acetylated Cam1-T6C; (3) Cam1-FRET; (4) Cam2; (5) IQ12 peptide (not used during this study); (6) Myo1IQ12-FRET; and (7) Myo1IQ12S742D-FRET.

DOI: https://doi.org/10.7554/eLife.51150.005

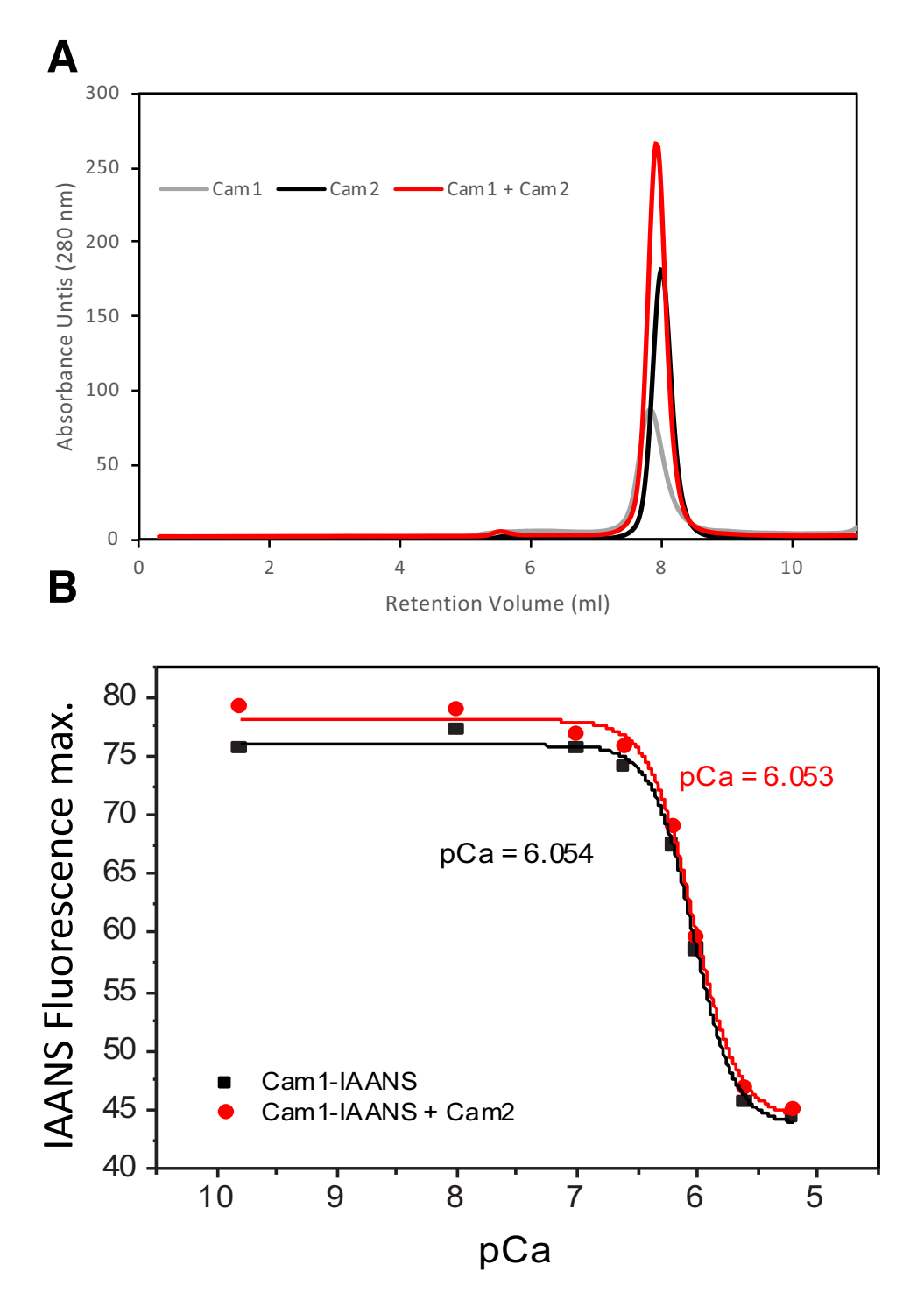

Figure 2—figure supplement 2. Cam1 and Cam2 do not interact directly. (**A**) Overlaid OD280 spectra of eluate from a Superdex 75 gel filtration column that had been loaded withCam1 (gray line), Cam2 (black line) or both Cam1 and Cam2 (red line) under identical 4 mM EGTA buffer conditions. (**B**) Maximum IAANS fluorescence values (440 nm) of 0.5 µM Cam1-IAANS over a range of pCa values. Black symbols show values for Cam1-IAANS, red symbols show values for Cam1-IAANS with 5 µM Cam2 protein. 2 mM Ca- EGTA buffers were used to give the indicated pCa values. pCa50 values were calculated from Origin fitting analysis - Hill equation.

DOI: https://doi.org/10.7554/eLife.51150.006

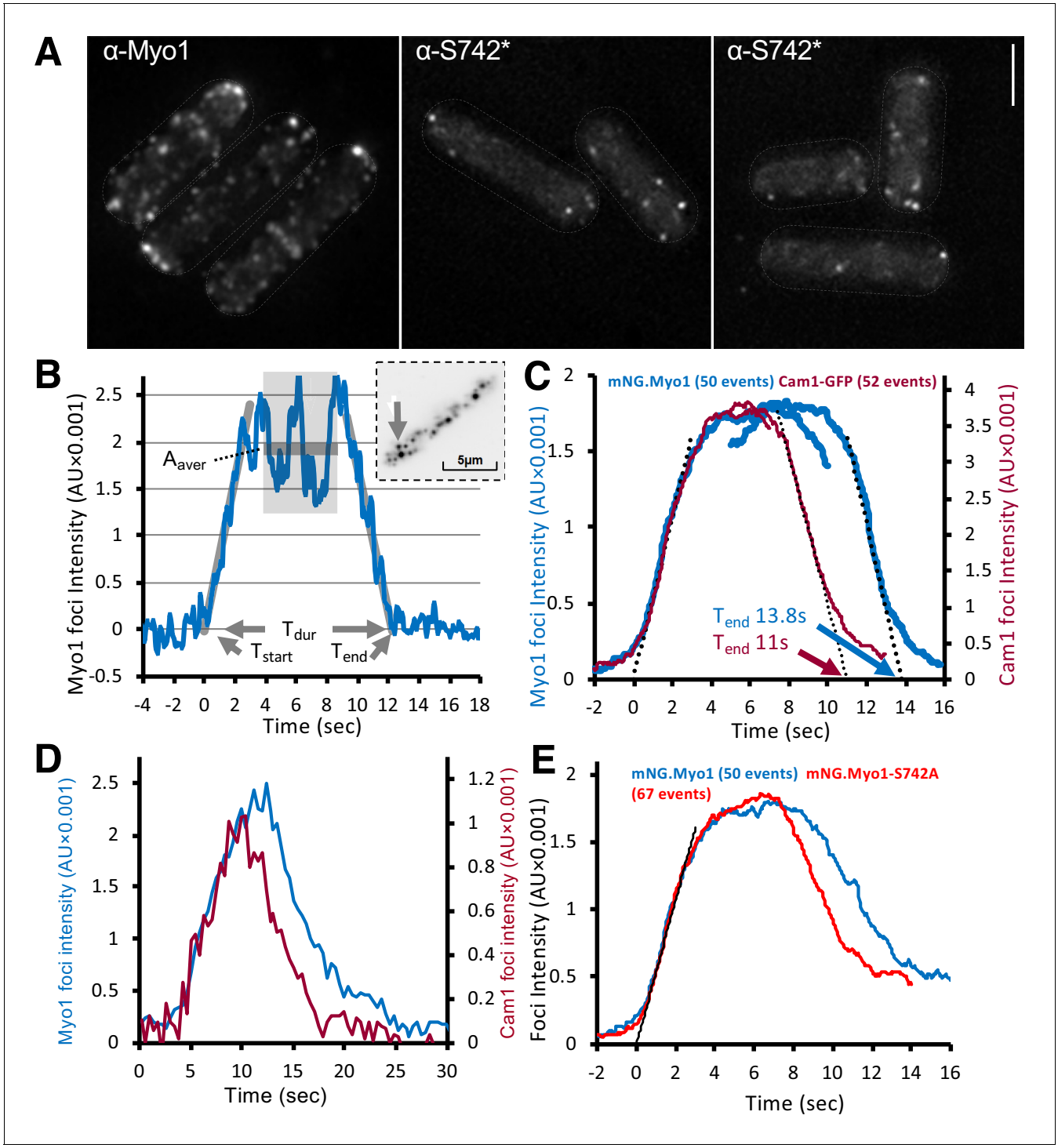

Figure 3. Myo1 and Cam1 dynamics in wild-type and *myo1.S742A* cells. (**A**) Maximum projections from 31-z stack widefield immunofluorescence images of wild-type cells, probed with anti-Myo1 (left panel) or anti-Myo1^{S742}* phosphospecific (right panels) antibodies, illustrate that S742 phosphorylated Myo1 localizes to cortical foci (scale bar, 5 μm). (**B**) An example relative-intensity trace of a single mNeongreen.Myo1 endocytic event. Linear fitting (grey lines, 60 points) was used to find the maximum gradient for both the rising and the falling slope. The intercept with zero intensity level was used to calculate T_{start}, T_{end}, and subsequently, the duration of the event T_{dur}. See detailed description in the Materials and methods section. Insert: an arrow highlights the analyzed endocytotic event (5 × 5 pixels area). (**C**) Averaged profile for individual Myo1 (blue) and Cam1 (red) membrane-association events, synchronized relative to T_{start} and T_{end}. Dotted lines show fitted rising (Myo1, 537 AU/sec; Cam1, 1073 AU/sec) and falling (Myo1, 567 AU/sec; Cam1, 1028 AU/sec) gradients. (**D**) An example fluorescence trace from simultaneous two-color imaging of a Myo1 (blue line) and Cam1 (red line) membrane-association event observed in *mNeongreen.myo1 cam1.mCherry* cells is consistent with the relative intensities and

Figure 3 continued on next page

Figure 3 continued

timings observed using single-fluorophore strains. (**E**) Averaged intensity trajectories of individual Myo1 (blue line) and Myo1.S742A (red line) endocytosis events from TIRFM imaging of *mNeongreen.myo1* and *mNeongreen.myo1.S742A* cells, respectively.

DOI: https://doi.org/10.7554/eLife.51150.007

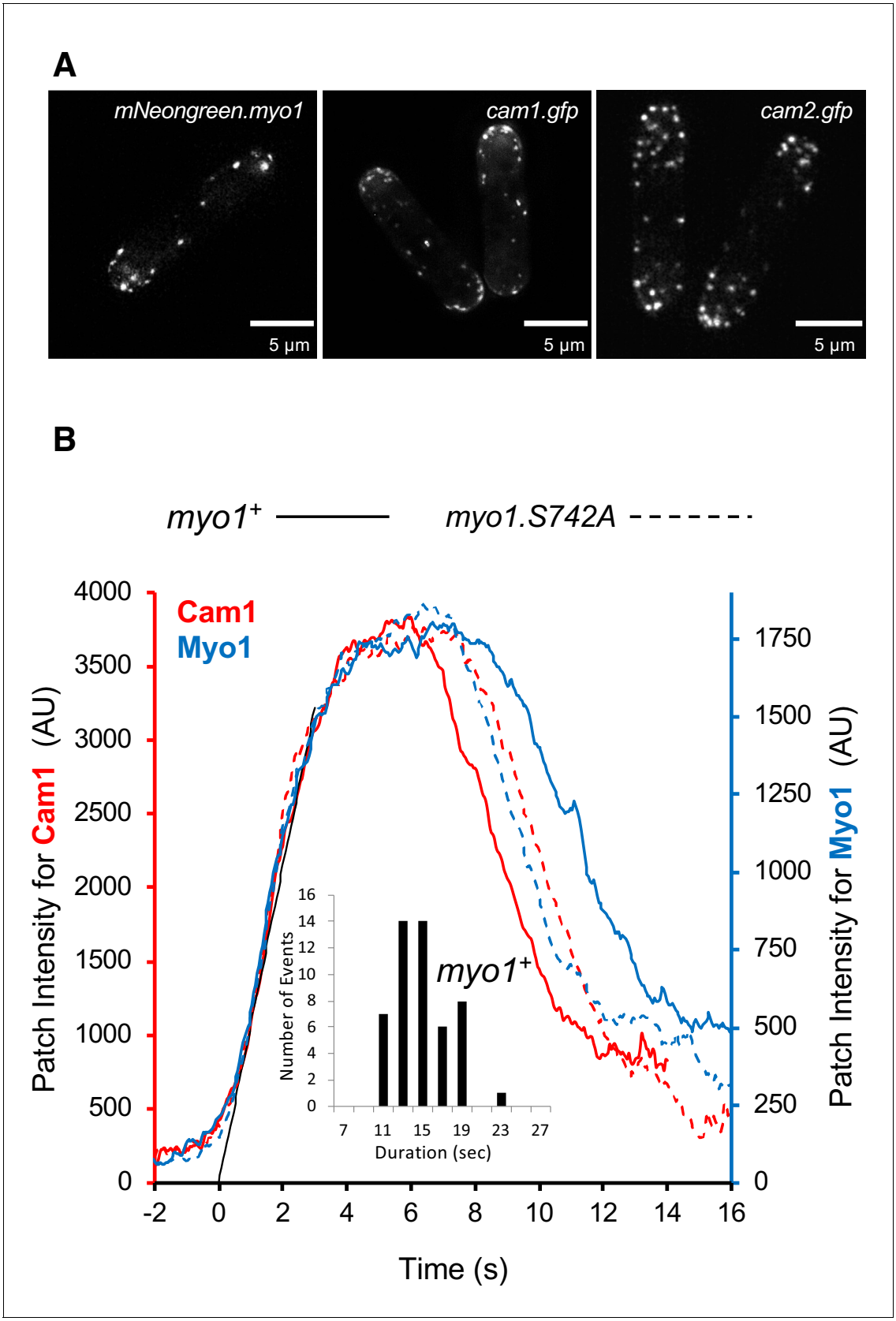

Figure 3—figure supplement 1. Relative TIRF profiles. (**A**) Maximum projections of 31-z stack widefield images of *mNG.myo1*, *cam1.gfp* and *cam2.gfp* cells (scales bars, 5 µm). (**B**) Combined profiles of averaged intensity trajectories of Myo1 (blue) and Cam1 (red) endocytosis events in wild-type (solid

Figure 3—figure supplement 1 continued on next page

Figure 3—figure supplement 1 continued

lines) or *myo1.S742A* strains (dashed lines). See Materials and methods section for the description of TIRF imaging. Insert: the distribution of the durations of individual wild-type Myo1 events.

DOI: https://doi.org/10.7554/eLife.51150.008

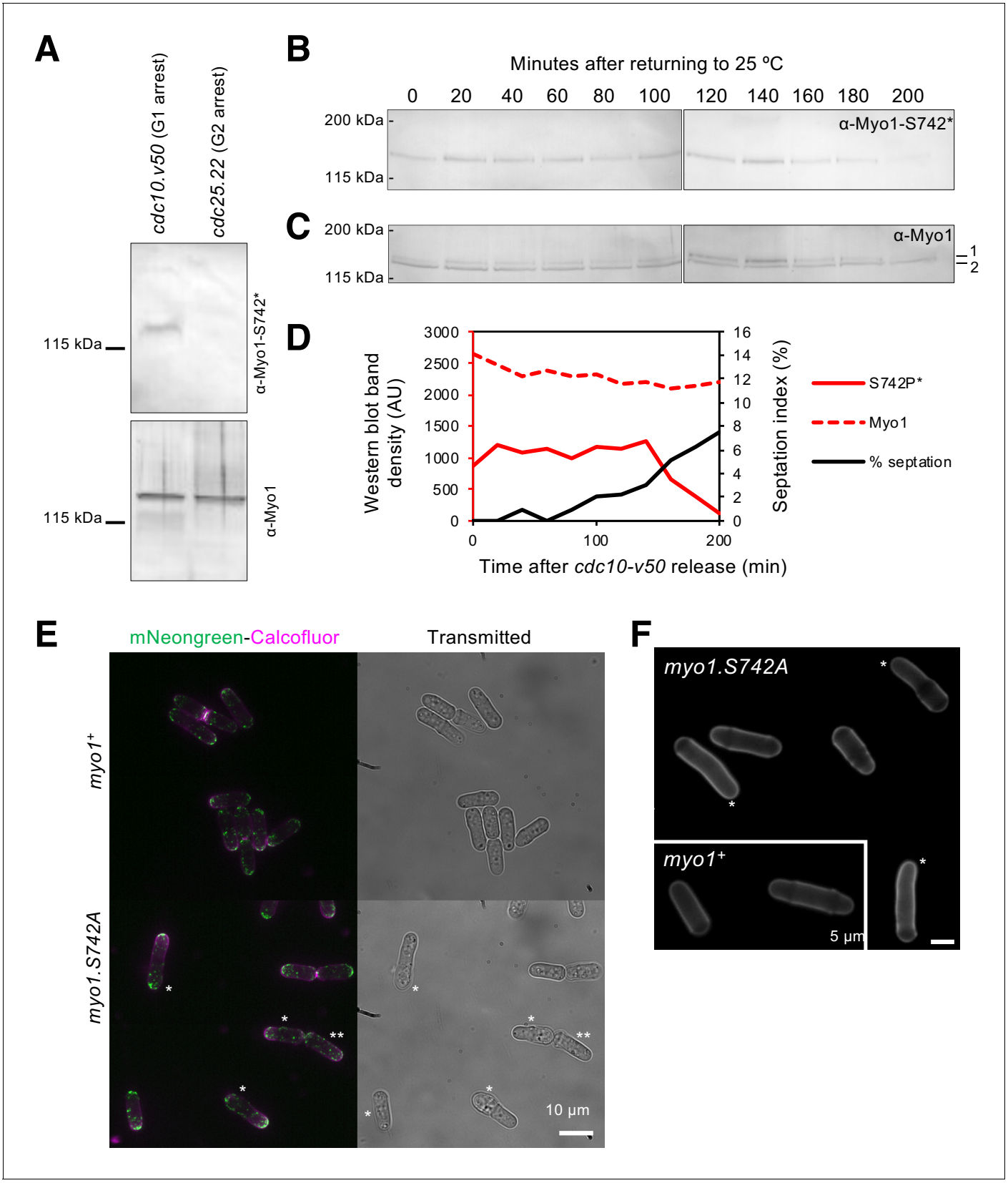

Figure 4. Myo1 S742 is phosphorylated in a cell-cycle-dependent manner to affect polarized growth. (**A**) Western blots of extracts from G_1-arrested *cdc10.v50* cells and pre-mitotic G_2-arrested *cdc25.22* cells probed with phospho-specific anti-Myo1^{S742} (upper panel) and anti-Myo1 (lower panel)

Figure 4 continued on next page

Figure 4 continued

antibodies demonstrate that Myo1 ^{S742} phosphorylation occurs before the Cdc10 execution point in monopolar G_1 cells, and is not detectable by the Cdc25 execution point at the end of G_2 (n = 3). (**B–D**) A *cdc10.v50* culture was synchronized in G_1 by shifting to 36˚C for 240 min before returning to 25˚C at time 0. Samples of cells were taken every 20 min from the release and processed for western blotting to monitor Myo1^{S742} phosphorylation. The membrane was first probed with phosphospecific anti-Myo1^{S742}* antibodies (**B**), and subsequently probed with anti-Myo1 antibodies to monitor total Myo1 (**C**). Both phosphorylated (1) and non-phosphorylated (2) Myo1 bands can be observed in panel (C). Equal loading was monitored by Ponceau staining of the membrane. (**D**) Densitometry measurements of phosphorylated Myo1^{S742} (from panel (B)) and total Myo1 (both bands from panel (**C**)) are plotted along with the % of cells in the culture with septa. (**E**) Myosin-1 distribution (green), calcofluor-stained regions of cell growth (magenta), and cell outline (transmitted image) of prototroph *mNeongreen.myo1*$^{+}$ and *mNeongreen.myo1.S742A* cells cultured in EMMG medium at 34˚C. Asterisks highlight cells that have morphology defects. Scale bar, 10 μm. (**F**) Calcofluor-stained WT and *myo1.S742A* cells. Asterisks highlight long bent cells displaying monopolar growth. Scale bar, 5 μm.

DOI: https://doi.org/10.7554/eLife.51150.011

A

	wt	*myo1.S742A*	*tea4Δ*	*cam2Δ*	*tea4Δ myo1.S742A*	*tea4Δ cam2Δ*
Average cell length (μm)	9.77	13.2	12.5	13.2	12.5	12.7
% Bent >5º off long axis	0.4	24.7	51.7	18.3	49.4	66.7
% multiple growth zones	0.0	0.0	5.7	0.0	4.6	18.9
n	>500	>500	88	83	88	91

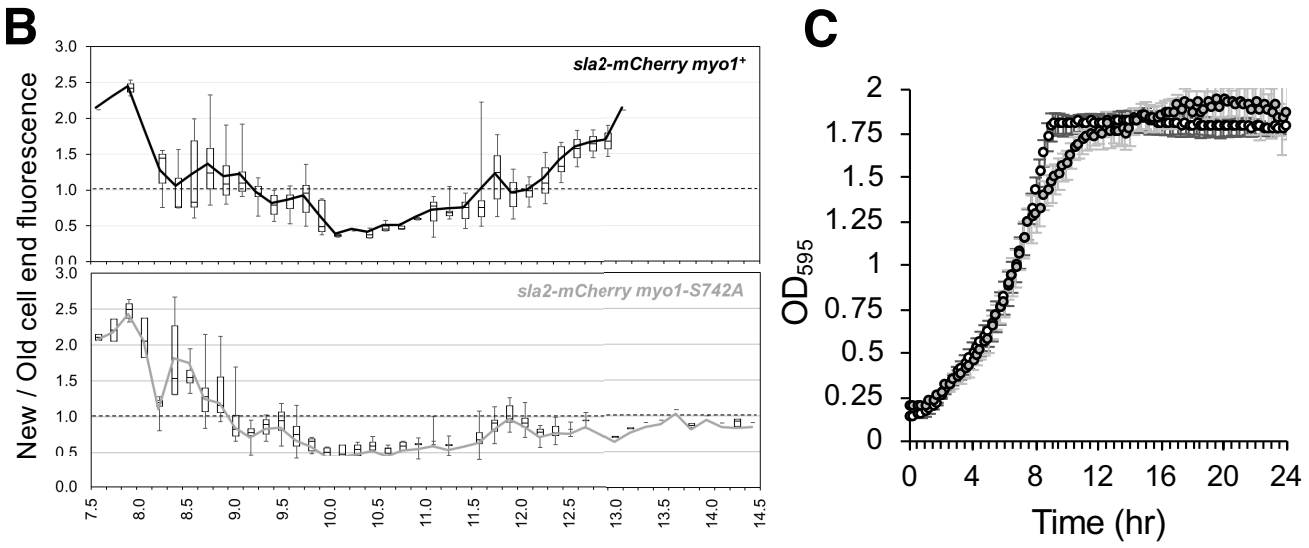

Figure 5. Myo1^{S742} phosphorylation impacts polarized cell growth. (**A**) Average length and frequency of growth defects in WT, *myo1.S742A*, *tea4Δ*, *cam2Δ*, *tea4Δ myo1.S742A*, and *tea4Δ cam2Δ* cells. (**B**) Ratio of Sla2-mCherry fluorescence at 'new':'old' cell ends, averaged from >30 growing mid-log *sla2-mCherry myo1*$^{+}$ (upper panel) and *sla2-mCherry myo1.S742A* (lower panel) cells. Boxes plots show the median and quartile for each length measured, whereas the lines are plots of the mean values at each length measured. (**C**) Averaged growth curves from three independent experiments of prototroph wild-type (empty circles) and *myo1.S742A* (gray-filled circles) cells cultured in EMMG medium at 34°C. Slower growth is apparent at the end of log phase in *myo1.S742A* cells, which grow more until reaching the stationary phase. Error bars denote the s.d. of the mean.

DOI: https://doi.org/10.7554/eLife.51150.012

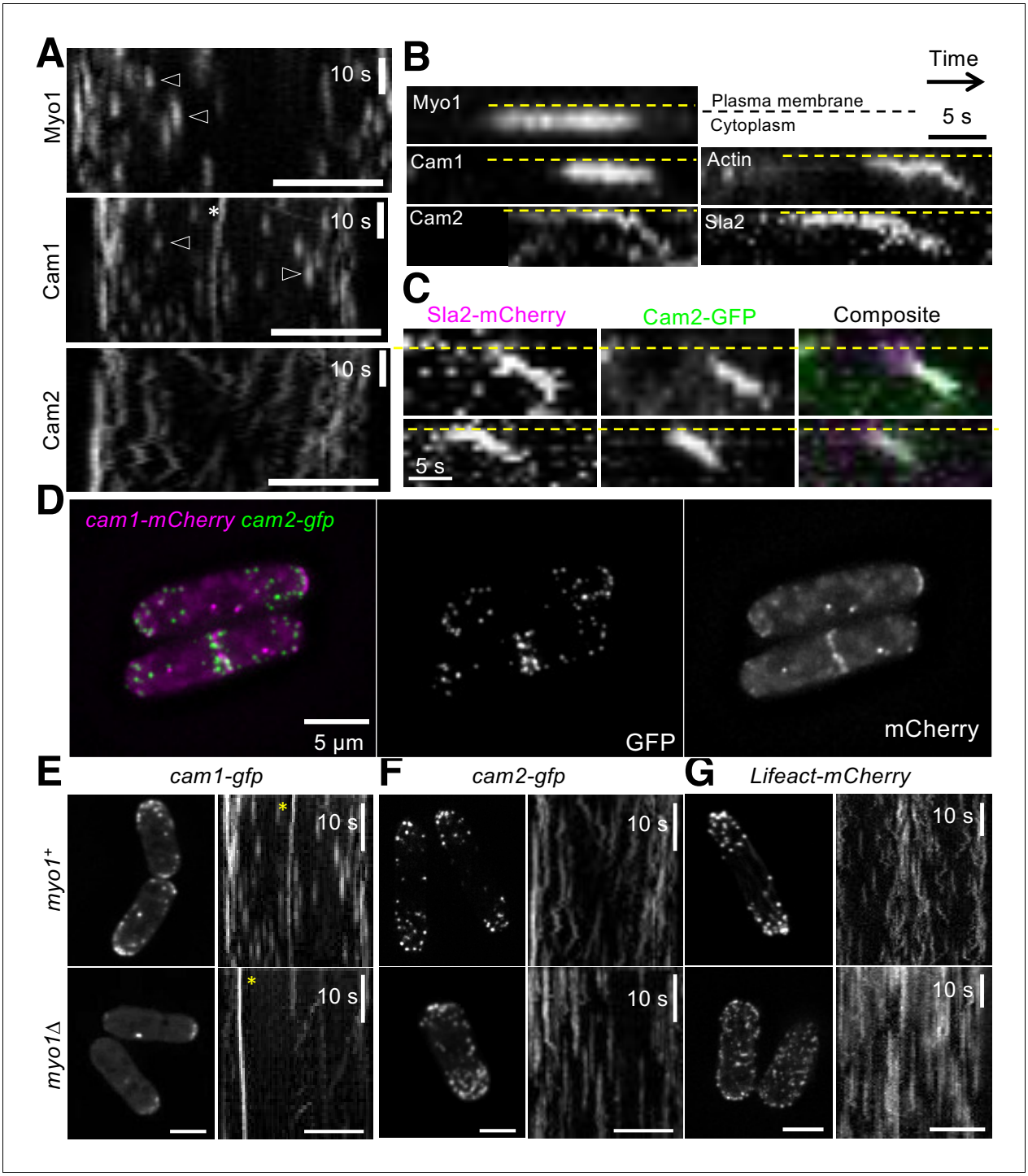

Figure 6. Cam2 associates with internalized endocytic vesicles. (**A**) Kymographs of GFP-labelled foci from maximum projections of 13-z plane time-lapse images of *mNeongreen.myo1* (upper panel), *cam1.gfp* (middle panel) and *cam2.gfp* (bottom panel) cells illustrate the static nature of Myo1 and Cam1 endocytic foci when associated with the plasma membrane (arrowheads). Cam1 foci that are associated with a spindle pole body (SPB) are highlighted. By contrast, Cam2 foci displayed extensive lateral movements. (**B**) Kymographs generated from single z-plane time-lapse images of single endocytic foci surfaces during vesicle formation and subsequent internalization. Myo1 and Cam1 only associate with the plasma membrane, whereas Cam2, Sla2 and actin are internalized on the vesicle after scission. These kymographs are not aligned temporally. (**C**) Kymographs of Cam2 and Sla2 co-internalization in *sla2.mCherry cam2.gfp* cells. (**D**) Maximum projection of a 31-z slice image of *cam1.mCherry cam2.gfp* cells reveals that Cam1 (magenta) and Cam2 (green) colocalize in a subset of endocytic foci. (**E–G**) Single frames (left panels) and kymographs (right panels) from maximum projections of 13-z plane time-lapse images of *cam1.gfp* (**E**), *cam2.gfp* (**F**) and *LifeACT.mCherry* (**G**) in either *myo1*$^{+}$ (upper panels) or *myo1*Δ (lower

Figure 6 continued on next page

Figure 6 continued

panels) cells. These images show that although only Cam1 recruitment to endocytic foci is dependent upon Myo1, the myosin is required for the internalization of Cam2-GFP and LifeACT.mCherry foci. Scale bar, 5 µm.

DOI: https://doi.org/10.7554/eLife.51150.013

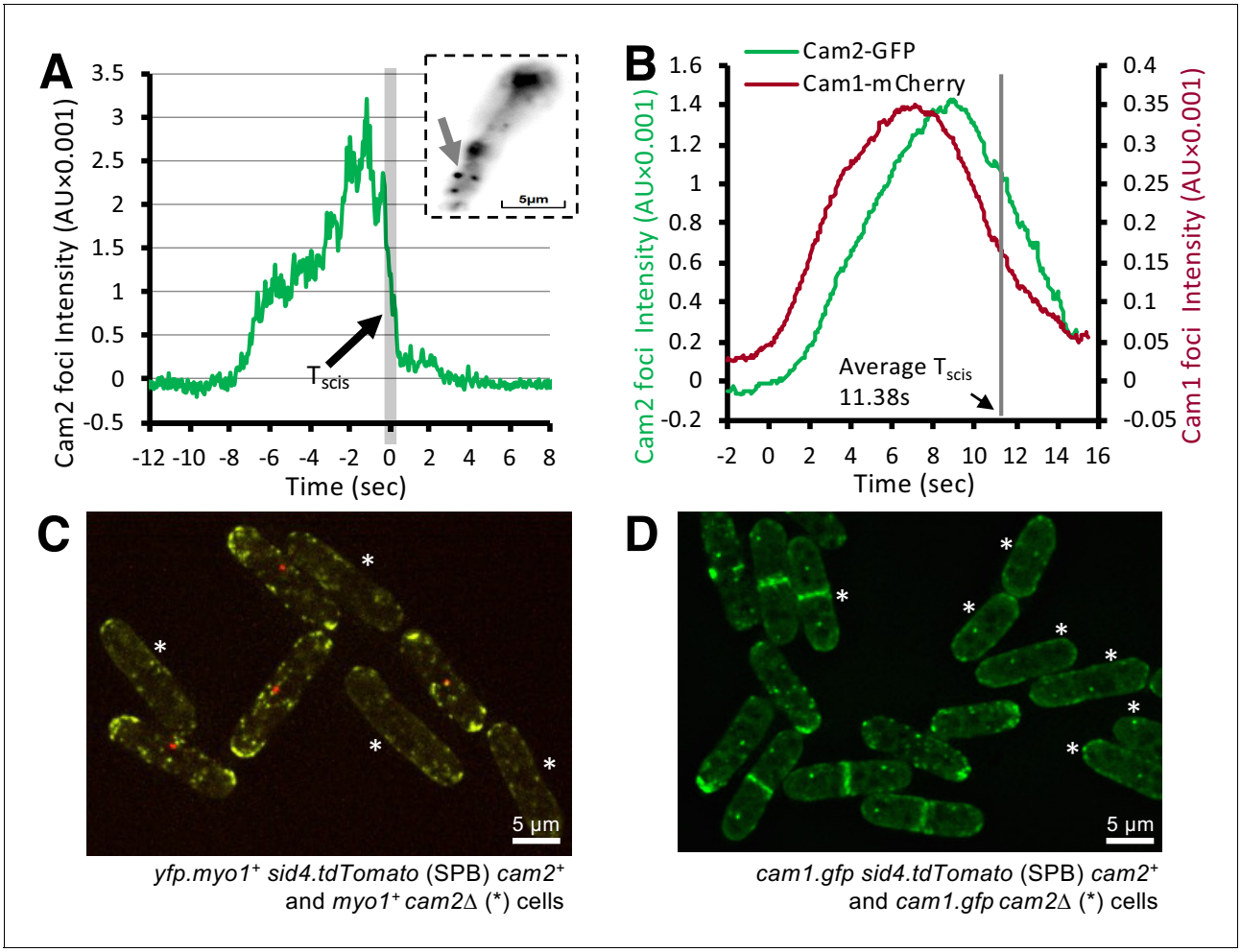

Figure 7. Cam2 does not impact Myo1 or Cam1 dynamics in vegetative cells. (**A**) An example fluorescence trace of a Cam2 membrane binding and vesicle internalization event from TIRFM imaging of *cam2.gfp* cells. An abrupt drop in the fluorescence was marked as 'scission time' (T_{scis}, gray vertical line). Insert: an arrow shows the location of the monitored endocytic event (5 × 5 pixels area). (**B**) Averaged profile from 65 individual Cam2 membrane association events (green line), together with the averaged Cam1-mCherry profile (red) from two-color TIRFM imaging of *cam1.mCherry cam2.gfp* cells. The events were synchronized relative to the Cam1 T_{start}. The gray line denotes the mean time of vesicle scission (T_{scis}). See detailed description in the Materials and methods section. (**C**) Maximum projection of a 31-z slice widefield image of a mixture of *yfp.myo1 sid4.tdTomato* (WT, with a red labeled SPB marker) and *yfp.myo1 cam2Δ* (asterisks) cells. Red-labeled SPBs allow differentiation between *cam2*$^+$ and *cam2Δ* cells in the same field. (**D**) Maximum projection of a 31-z slice widefield image of a mixture of prototroph *cam1.gfp sid4.tdTomato* (WT, with a red-labeled SPB marker) and *cam1.gfp cam2Δ* cells (asterisks). Red-labeled SPBs allow differentiation between *cam2*$^+$ and *cam2Δ* cells in the same field. Scale bars, 5 µm.

DOI: https://doi.org/10.7554/eLife.51150.014

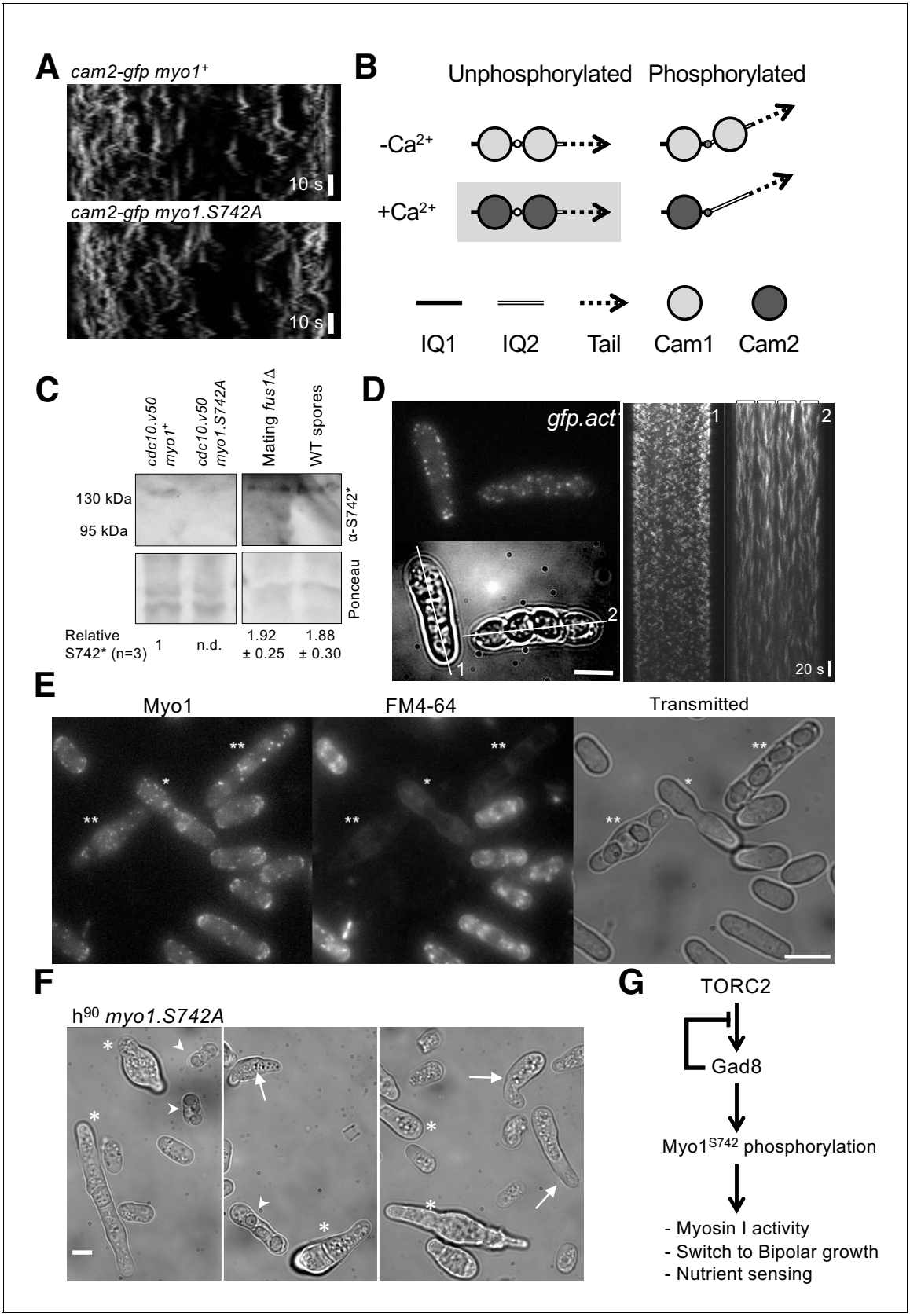

Figure 8. Myo1 S742 phosphorylation regulated Cam1 and Cam2 dynamics during meiosis. (**A**) Kymographs of Cam2.GFP foci dynamics in *myo1*$^{+}$ (upper panel) and *myo1.S742A* (lower panel) cells. (**B**) Scheme of the consequences of phosphorylation of Myo1^{Ser742} (small empty circle) and Ca^{2+}

Figure 8 continued on next page

Figure 8 continued

levels upon the binding of Cam1 (light gray filled circle) and Cam2 (dark gray filled circle) to the IQ1 (solid thick black line) and IQ2 (double line) motifs of Myo1, and the impact on the relative orientation of the myosin lever arm (dashed arrow). The highlighted combination of unphosphorylated Myo1^{S742} and Ca^{2+} does not normally occur in cells. (**C**) Western blots of extracts from G_1-arrested *cdc10.v50 myo1*$^+$, *cdc10.v50 myo1-S742A*, and conjugation arrested (starved, premeiotic cells) *fus1*Δ cells, and from meiotic spores, probed with phospho-specific anti-Myo1^{S742} antibodies (upper panel). Ponceau staining (lower panel) confirms that Myo1S742 remains phosphorylated from the end of G_1, through conjugation until the end of meiosis (n = 5). Relative Myo1^{S742} phosphorylation levels were calculated from three independent equivalent experiments (mean ± sd). (**D**) Left panel: maximum projection of a 13-z slice GFP fluorescence image (top) and a transmitted light image (bottom) from a time-lapse of vegetative (cell 1) and meiotic (cell 2) *gfp-act1* cells. Image from a GFP-act signal. The kymographs in the right panels were generated along the two dotted axes. (**E**) Maximum projection of mNeongreen-Myo1 fluorescence (left), FM4-64 fluoresence (middle) and transmitted light images of a mixed population of vegetative, fusing (*) and sporulating (**) *mNG-myo1*$^+$ cells, illustrating that endocytosis is reduced in meiotic cells. Scale bar, 10 μm. (**F**) Micrographs illustrating *myo1.S742A* cell morphology on solid starvation medium. Asterisks highlight cells with unregulated growth and polarity defects; arrows highlight cells with elongated or abnormally bent shmooing (conjugation) tips; arrow heads highlight meiotic cells with defective spore formation. Scale bar, 5 μm. (**G**) A schematic of the TORC2–Gad8–Myo1^{S742} signaling pathway.

DOI: https://doi.org/10.7554/eLife.51150.017